(2)

Studies on Atmospheric Mixed Layer

Minoru GAMO

主論文1

Seasonal Change of the Mixed Layer Structure at Tsukuba

By Minoru Gamo

Reprinted from the Journal of the Meteorological Society of Japan
Vol. 63, No. 1, February 28, 1985

Seasonal Change of the Mixed Layer Structure at Tsukuba

By Minoru Gamo

National Research Institute for Pollution and Resources,
Ministry of the International Trade and Industry, Yatabe, Tsukuba, Ibaraki 305, Japan
(Manuscript received 9 August 1984, in revised form 23 November 1984)

Abstract

The integrated surface sensible heat flux and the maximum mixing depth are obtained by routine aerological data and daily maximum and minimum temperature data measured at the Tateno Aerological Observatory located 60 km east of Tokyo. Annual variations of the components of the surface heat balance are also estimated from the integrated surface heat flux, net radiation and the downward flux of short-wave radiation. Annual variations of the convective velocity scale, the standard deviation of the vertical velocity fluctuations, and the eddy diffusivity are estimated by the surface heat flux and mixed layer height. The potential temperature gradient of the stable layer capping the mixed layer is 0.003°C/m during the winter season, 0.005°C/m in midsummer, and 0.003°C/m under the travelling anticyclones. The integrated surface sensible heat flux from sunrise to a time when the daily maximum temperature occurs is largest in early spring (170 ly), smallest in winter (50 ly). The maximum mixing depth is highest in March (1,500 m) and lowest in December (700 m). The surface sensible heat flux is largest in spring because of low temperatures, aridity, and a small amount of evapotranspiration. The Bowen ratio is unity in May and November. The lowest value of the Bowen ratio is 0.4 in July. Agreement of the above-mentioned values with more accurate observations is reasonably high. So this simple method for estimating parameters of the mixed layer structure is ascertained to be useful.

1. Introduction

The vertical distribution of the tropospheric temperature shows a slightly stable stratification resulting from radiative cooling and water vapor. On warm, sunny days, the surface inversion layer formed by nocturnal radiation and the above-mentioned stable layer are gradually destroyed from the surface by thermal free convection caused by surface heating by the sun.

In this paper, annual change of the mixed layer structure is estimated by a temperature profile from an aerological observation, and daily minimum θ_{min} and maximum temperatures θ_{max}. For analysis, an encroachment model (a model where entrainment is not considered) is used. From the above three data, the lapse rate of the upper stable layer capping the mixed layer γ, the maximim mixing depth MMD, the diurnal temperature range, $\Delta\theta$, and turbulent sensible heat flux from the earth's surface H_0 are obtained. Surface heat flux H_0 is calculated by an area enclosed by potential temperature profile $\theta(z)$, θ_{min}, and θ_a ($=\theta_{max}-2$°C) in the $\theta-z$ plane. (The reason we use θ_a is described later.) Calculated values of H_0 are integrated values taken from just before sunrise when minimum temperatures are measured to a time maximum temperatures are reached. This method is hereafter simply referred to as the profile-integrated method.

The value of H_0 is generally obtained by the eddy correlation method or an aerodynamic method, such as, the gradient or bulk method. High grade techniques are necessary for the eddy correlation method, while for the aerodynamic method, eddy coefficient and many other parameters which vary with meteorological, geographical conditions etc. are assumed.

On the other hand, the profile-integrated method gives direct integrated H_0 values supplied from the surface to the mixed layer. Thus, this method has no empirical parameters and is easy to estimate. Aerological data are necessary for this method, and the estimated H_0 values have representative features which cover a comparatively wide area compared with the before-mentioned methods. Annual and regional changes of the mixed layer structure are also easily estimated. Seasonal variations of energy balance and the intensity of convective activities are evaluated by the surface sensible heat flux obtained by this method.

According to the encroachment model (e.g., see Gamo and Yokoyama, 1979), the mixed layer structure: mixing depth, constant potential temperature through the mixed layer, and turbulence quantities are determined by surface heat flux H_0 and the lapse rate of the upper stable layer γ. Therefore, if the annual variations of $\gamma(z)$ which is assumed to be constant during a day and diurnal course of H_0 are known, seasonal variations of the daily mixing depth variance and the spatial and time variations of turbulence, eddy diffusivity, etc. can be obtained.

Pollutants emitted from the surface such as smokestacks, cars, etc. are mixed vertically in the mixed layer, and materials which cause air pollution, such as ozone, are pulled into the mixed layer. Thus, the annual variations of the mixed layer structure may be useful for seasonal simulation of air pollution. Rough estimation of the mixed layer structure is effective for planning refined boundary layer observations. Besides, the seasonal variation of the mixed layer has influenced the people's way because people live near the bottom of the mixed layer.

2. Estimation of surface heat flux and correction of errors

For the encroachment model, the relationship between the potential temperature increment through the mixed layer $d\theta$ in the time interval dt, and the surface sensible heat flux H_0 is described as

$$H_0 dt = \rho C_p h_m d\theta , \qquad (1)$$

where h_m is the mixing depth, ρ the mean air density in the mixed layer, C_p the specific heat of air at constant pressure. Assuming the constant potential temperature through the mixed layer increases from θ_1 to θ_2 in the time interval t_1 to t_2, the following equation is derived:

$$\int_{t_1}^{t_2} H_0 dt = \rho C_p \int_{\theta_1}^{\theta_2} h_m(\theta) d\theta , \qquad (2)$$

where ρ (1,250 g/m^3) and C_p (0.24 cal/g K) are assumed to be constant with height and time.

As illustrated in Fig. 1, the initial stable layer described by the potential temperature profile is eroded from the surface and the mixed layer develops. Thus, the lined area enclosed by the potential temperature profile represented by $\gamma(z)$, θ_1, and θ_2, and multiplied by ρC_p gives the integrated surface heat flux supplied from the surface in the time interval between t_1 and t_2.

It is assumed the mixed leyer is rapidly mixed. If the mixed layer is mixed instantaneously, the value of H_0 can be estimated. In reality, only the value of H_0 averaged over a period of time (one hour or more) seems to be meaningful.

Willis and Deardorff (1974) and Yoshikado (1980) calculated surface heat flux from the temperature profile in a water tank and channel, respectively.

Replacing t_1, t_2, θ_1 and θ_2 with t_i (time of sunrise), t_a (time when temperature becomes

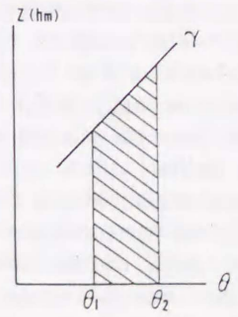

Fig. 1 Relationship between potential temperature in the mixed layer $\theta(z)$, mixed layer height h_m, and lapse rate γ. The lined area shows integrated surface sensible heat flux.

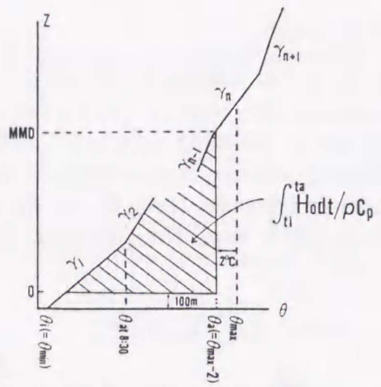

Fig. 2 Relationship between maximum mixing depth MMD, γ, and integrated surface heat flux $\int_{t_i}^{t_a} H_0 dt$. A time lag of radiosonde thermometer is assumed to be 100 m. The maximum potential temperature θ_a in the mixed layer is assumed to be $(\theta_{max}-2°C)$.

θ_a), θ_i and θ_a, respectively, equation (2) becomes:

$$\int_{t_i}^{t_a} H_0 dt = \rho C_p \int_{\theta_i}^{\theta_a} h_m(\theta) d\theta , \qquad (3)$$

where the units are: H_0[cal/(m² s),], h_m[m], θ[K], θ_i[K], θ_a[K], t[s].

A scheme of the relationship between θ_i, θ_a, and the potential temperature profile represented by γ is shown in Fig. 2. The lapse rate γ is obtained from a temperature humidity significant level tables of the aerological data.

Pressure height in the aerological data is replaced with height z (in meters) from the pressure-height equation. Temperatures of the aerological data are replaced with potential temperatures (°C) from the equation $\theta = T + \gamma_d z$, where γ_d is the dry adiabatic lapse rate (0.0098°C/m). The values of θ_a, and θ_i are assumed to be the same as the potential temperatures because θ_{max} $(=\theta_a+2°C)$ and θ_i are observed near the surface in the instrument screen shelter.

Rawinsonde is emitted at 8:30 every morning at the Tateno Meteorological Observatory (36°03′N, 140°08′E, 25.5 m above sea level). Therefore, the potential temperature profile at sunrise is unknown. Here, we adopt the minimum temperature θ_{min} as a lower boundary θ_i in the integration of the right side of equation (3) and assume θ_{min} to be equal to the air temperature at sunrise. In Fig. 2, we connected the point represented by θ_i with the first kink height from the surface of the potential temperature and assumed the line obtained by the procedure described above to be the potential temperature profile at sunrise in the lowest layer. The potential temperature profile above the first kink height is assumed to be the same as sunrise. It is assumed that this profile is eroded by the developing mixed layer. The temperature θ_a is defined as the maximum value of the potential temperature in the mixed layer and is assumed to be constant regardless of its height in the mixed layer.

Thus, the area enclosed by the potential temperature profile, θ_i and θ_a equals $\frac{1}{\rho C_p}\int_{t_i}^{t_a} H_0 dt$, the integrated surface heat flux divided by ρC_p from sunrise to the time when the daily temperature near the surface reaches its peak value.

According to Gamo *et al.* (1983), the relationships between MMD, H_0, and the potential temperature profile which consists of n stable layers are as follows:

$$\mathrm{MMD} = \left(\frac{2}{\rho C_p}\sum_{j=1}^{n}\frac{1}{\gamma_j}\int_{t_{j-1}}^{t_j} H_0 dt\right)^{1/2}, \qquad (4)$$

where $t_0=t_i$, $t_n=t_a$, γ_1 is the lapse rate of the lowest stable layer (surface inversion layer), and γ_n the lapse rate at the height of the maximum mixing depth. Integrated H_0 can be obtained by equation (3), or by an area enclosed by the potential temperature profile at sunrise, θ_i $(=\theta_{min})$, and θ_a, consists of the combination of a triangle and trapezoids.

The error of the integrated heat flux obtained by the above method was checked. First, a bimetal thermometer with a large time lag is attached to the rawinsonde. Yamamoto (1975) theoretically estimated the thermometer time lag to be about 80 m. Suzuki *et al.* (1977) obtained a time lag of about 100 m by comparing rawinsonde and kite balloon observations. Here, it is assumed that rawinsonde temperature data equals the temperature at a height of 100 meters below a certain tabled altitude in the aerological data. Second, the lowest layer of the mixed layer is unstable.

Thus in general, the daily maximum temperature is higher than the constant potential temperature of the mixed layer. Also, the daily maximum temperature θ_{max} seems to show the largest instantaneous value, because θ_{max} is measured by a maximum and minimum thermometer. From a comparison of θ_{max} and the constant potential temperature θ_a within the mixed layer measured by rawinsonde at 14:30 JST at Tateno, θ_a is lower than θ_{max} by about 2°C. Lee (1983) and Lee and Hanafusa (1984) showed by low-level rawinsonde observations above the site of the Meteorological Research Institute situated in the same area as the Tateno Aerological Observatory that the temperature near the surface is 1.6–1.7°C higher than the constant potential temperature throughout the mixed layer. They also found that the MMD calculated by the surface temperature becomes higher than the real MMD at Tateno. Therefore, the constant potential temperature θ_a within the mixed layer when the mixed layer develops up to MMD is assumed to be θ_{max} −2°C. An unstable layer near the surface is neglected. Fig. 2 shows the calculation method of the integrated surface sensible heat flux and MMD, considering the above mentioned correction for the two errors.

Carson (1973) estimated the time change of the mixed layer for the temperature jump model. Deardorff (1979) presented the real mixed layer model. However, these models are too complicated for application to the real daily change of the mixed layer because the more accurate the mixed layer model becomes, the larger the necessary number of parameters for the mixed layer, such as the entrainment parameter A $(=-H_i/H_0$, H_i is the negative heat flux at the mixed layer height) becomes. The structure near the mixed layer height is complicated and there is no sufficient model at present. Also, errors due to advection, subsidence, and air mass modification may affect the results of analyses. The integrated surface heat flux H_0 is overestimated by subsidence, and air mass modification of the anticyclones. The value of H_0 in the above-mentioned entrainment, and advection of the cold atmosphere, such as sea breezes are underestimated. Since errors are not clear, the above errors are assumed to be negligible in this paper.

3. Data

Annual variations of the mixed layer above Tateno were analyzed. Tateno is located in the center of Tsukuba Science City, 20 km south of Mt. Tsukuba, 10 km west of Lake Kasumigaura, and 40 km west of the Pacific Ocean. Tateno is surrounded by pine groves, cultivated fields, rice paddies, and rural houses. Since about 1978, multi-storied buildings and wide streets have been constructed around Tateno. An analysis was made for a fifteen year period from 1967 to 1981. The fair weather days when the mixed layer is well developed were selected from the routine meteorological observations at the Tateno Aerological Observatory (tabulated in the Monthly Weather Bulletin of Ibaraki Prefecture), on the following three conditions. First, the duration of sunshine was larger than 75% of the maximum (averaged 15 years) in the month. Second, the daily mean wind velocity was less than 3 m/s. Third, there was no daily precipitation.

The typical mixed layer where there is no wind velocity gradient does not exists in the real atmosphere. However, the mixed layer model may be applied to warm, sunny days with slight breezes. A fifteen year total of 1164 warm, sunny days, and an average annual mean total of about 78 means that a typical mixed layer develops for one day per five days on the average.

The following three weather types are predominant for the mixed layer developing days as shown in Fig. 3. First is the winter type (W) during the winter monsoon. The winter weather is governed by the cold Siberian air mass (P_c) modified during its path across the Japan Sea and the central ridge of the Japanese Islands. Fine weather prevails in districts on the Pacific Ocean side of Japan, as opposed to the snowy weather on the Japan Sea side. Second is the summer type (S) under the influence of the subtropical air mass locally called the Ogasawara Anticyclone (T_m) which consists of wet, very warm air. Third is the

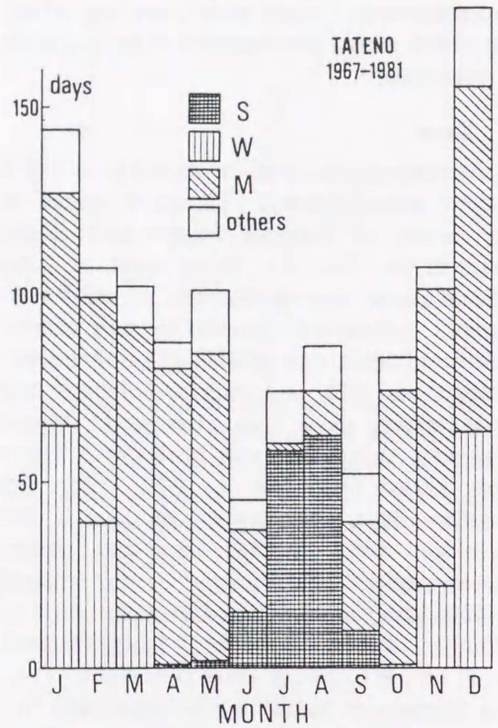

Fig. 3 Annual variations of numbers of the mixed layer days; W, during the winter monsoon; S under the Ogasawara High; M, during the migratory anticyclone path across the Japan Islands.

migratory anticyclone type (M). Migratory anticyclones that are cut-off anticyclones from the Yangtze River air mass (T_c) prevail especially in spring and autumn. (A more detailed description about the climate of Japan is given in Fukui, 1977). As shown in Fig. 3, fair weather days with light winds are mainly grouped into the above three types. Other fair weather types are shown in Gamo (1983).

The number of days when a mixed layer developes is large in winter and small in summer. Predominant fair weather for each month is classified into four groups: (1), types W and M are predominant in the winter season from November to February, (2), type M dominates in March, April, and October, (3), type S prevails in midsummer, (4), types S and M are predominamt in June and September.

4. Lapse rate of the upper stable layer

As mentioned before, the lapse rate of the upper stable layer capping the mixed layer is an important parameter in determining the mixed layer structure. Also, γ is the parameter determining the frequency of the Brunt Väisälä frequency, mountain waves, gravity waves, etc. The value of the upper stable layer γ is thought to be determined by the complex combination of the meteorological, geographical and topographical conditions. Here, we investigated the relationships between the value of γ and a prevailing air mass or its modification.

The monthly mean of the potential temperature profile up to a height of 4 km above the surface is shown in Fig. 4. Roughly speaking, each potential temperature profile is almost parallel except during June which is the rainy season. Profiles on fair weather days of April and May are similar to those of November and October, respectively.

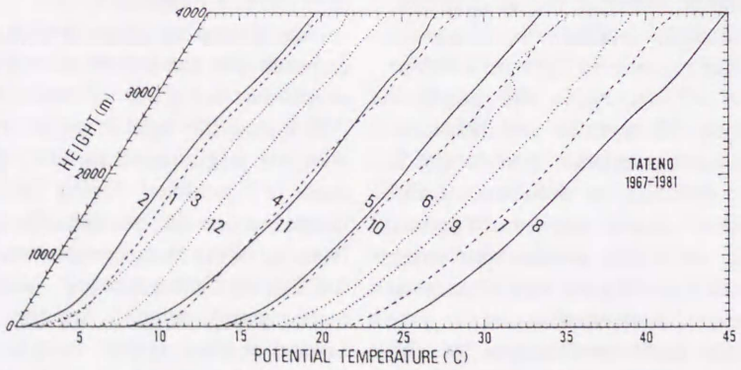

Fig. 4 Monthly mean of the potential temperature profile at sunrise up to a height of 4 km above the surface for days when the weather is fair and the mixed layers are well developed. Profile labels give months.

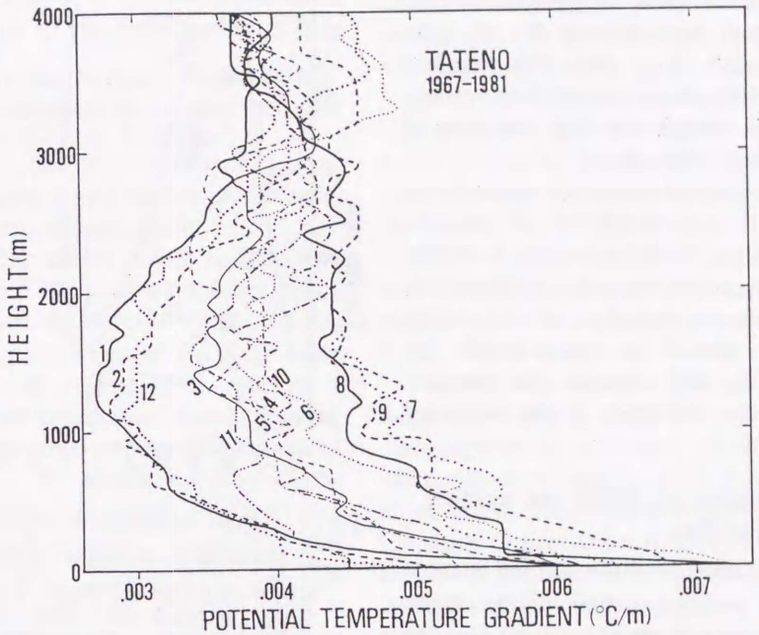

Fig. 5 Same as Fig. 4, but for potential temperature gradient.

Figure 5 shows the monthly mean potential temperature gradient up to a height of 4 km above the surface averaged over a fifteen year period. Lapse rate γ above a height of 3 km does not change throughout the season, and its value corresponding to 5.5-6°C/(100 m) as a value of the temperature lapse rate is nearly equal to that of the standard atmosphere. On the other hand, γ greatly changes below a height of 2 km where a mixed layer developes. Annual variations of γ are classified clearly into the following three types: first, the winter season type for winter months from December to February; second, the summer season type including early fall from July to September; third, the spring and autumn type from March to June, and October and November. The values of the lapse rate γ at 1000 m are as follows: 0.003°C/m in winter, 0.005°C/m in summer, and 0.004°C/m in spring and autumn. Seasonal change of γ corresponds with observed changes obtained by the difference of temperatures between mountain summits and bases summarized by Yoshino (1975). The fair weather days under the travelling anticyclones which appear throughout the season are shown in Fig. 6. The value of γ during the winter from December to February is about 0.003°C/m and 0.005°C/m from July to September. In summer, the number of migratory anticyclones is very small, and in winter the value of γ is nearly the same as that of the winter monsoon. The reason for this is probably because the winter monsoon originates in the Siberian continental

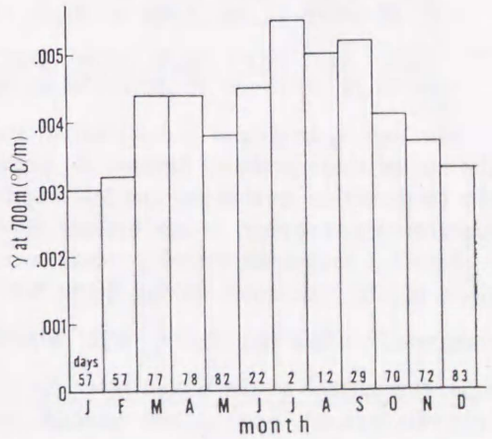

Fig. 6 Monthly mean of the potential temperature gradient at a height of 700 m for the mixed layer in the case when the migratory anticyclones bring out a fair weather.

anticyclone, and travelling anticyclones in this season are cut-off anticyclones of the continental air mass. Two other fair weather patterns: S and W are specific to their respective seasons, so we can say that the value of γ is characteristic of a season.

One parameter determining the mixed layer structure, γ, is repreeentative of season. Another parameter, surface sensible heat flux H_0 has, of course, climatological characteristics. Therefore, seasonal variation of the mixed layer structure should be characteristic for each season. We will describe the monthly mean mixed layer structure in the following section.

5. Annal variation of MMD and surface sensible heat flux

The seasonal change of the surface sensible heat flux H_0, and maximum mixing depth which is determined mainly by H_0 and the lapse late above the mixed layer were examined. According to the hourly surface AMeDAS (Automated Meteorological Acquisition System) data for a four year period from 1978 to 1981 of Shimotsuma 15 km northwest from Tateno, the annual mean time t_a when the daily maximum temperature θ_{max} appeared was 13:55 JST for the days when the mixed layer developed. The monthly means of time t_a are as follows:

JAN	FEB	MAR	APR	MAY	JUN
13:55	14:05	14:10	14:00	14:20	13:45

JUL	AUG	SEPT	OCT	NOV	DEC
13:55	13:20	13:35	13:40	13:35	14:00

The time t_a in August is much earlier than the annual mean probably because in August the condensation level is low and fair weather cumulus clouds appear, or sea breezes blow.

Figure 7 shows the monthly mean variations of the maximum mixing depth MMD, integrated surface heat flux $\int_{t_i}^{t_a} H_0 dt$ supplied from the surface to the mixed layer for time intervals between t_i and t_a, and potential temperature gradients of the stable layer at a height of MMD-100 m above the surface. The height MMD-100 m was selected because the mixed layer does not develop up to this height at 8:30 JST when rawinsonde measurement begins, the surface strong inversion layer does not reach this height, and the maximum mixing depth becomes higher than this height.

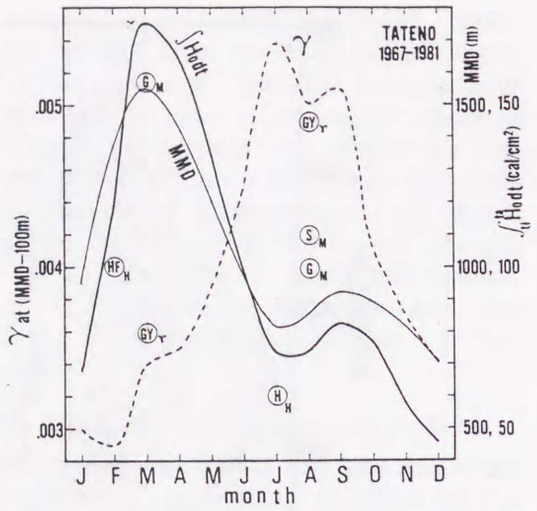

Fig. 7 Annual variations of MMD, γ at a height of MMD-100 m at sunrise, and $\int_{t_i}^{t_a} H_0 dt$. Observed values are as follows: Symbol GY shows Gamo and Yokoyama (1979); G, Gamo *et al.* (1976); S, Sasano *et al.* (1983); H, Hanafusa *et al.* (1978); HF, Hanafusa and Fujitani (1979). Suffixes γ, M, and H show potential temperature gradient, MMD, and integrated surface heat flux, respectively.
1 cal/cm²=4.19×10⁻² MJ/m².

Since Holzworth (1964) first obtained MMD from temperature profiles and θ_{max}, many researchers have obtained MMD at many sites. In this paper, we use $\theta_{max}-2°C$ as the constant potential temperature θ_a within the mixed layer.

The maximum mixing depth MMD at Tateno is about 1,500 m from late winter to early summer, 800 m in midsummer, a little higher in autumn, and lowest in winter (700 m).

As mentioned before, the lapse rate of the stable layer above the mixed layer γ is lowest in the winter season (0.003°C/m), increases gradually in spring, is highest from July to September (0.005°C/m), and decreases rapidly in autumn.

The integrated surface sensible heat flux

$\int_{t_i}^{t_a} H_0 dt$ is largest in the early spring (170 ly =7.1 MJ/m²), small in summer (70 ly=2.9 MJ/m²), larger in autumn than in summer, and lowest in winter (50 ly= 2.1 MJ/m²).

As shown in (4), the maximum mixing depth MMD is determined by two parameters, γ and H_0. The integrated surface heat flux shows a relatively wide range with values ranging from 50 to 170 ly. On the other hand, γ changes from 0.003 to 0.005°C/m. Therefore, in this study the value of H_0 plays more important role in determing MMD than γ.

Results of observations are also plotted for comparison in Figure 7. Symbol GY represents the lapse rate γ for March and August obtained by the airborne measurements over the northern surrounding area of Tokyo (Gamo and Yokoyama, 1979). The values of γ in this study agree very well with observed ones.

Observed results of the sensible heat flux H_0 around Tsukuba were obtained by the eddy correlation method. Hanafusa and Fujitani (1979) (Symbol HF in Fig. 7) observed 100 cal/cm² in February, and Hanafusa *et al.* (1978) (Symbol H) measured 60 cal/cm² in July. These results are read roughly from the graph of the daily variations of H_0 from sunrise to about 14 JST. These observational results have the same tendency of the H_0 variation shown in Fig. 7.

Finally, symbol G shows the MMD obtained by the airborne measurements over the Kanto Plain (Gamo *et al.*, 1976). Symbol S shows MMD obtained by laser observations at Tateno at about 14 JST by Sasano *et al.* (1983). The values of MMD in this study are slightly lower than those for August. For the ideal temperature jump model, if we assume the generally accepted entrainment parameter A ($=-H_i/H_0$) to be 0.2, MMD by aerological data becomes about 1.2 times larger than that in Fig. 7 (see Gamo *et al.*, 1983), and corresponds with observations. Anyway, the MMD in Fig. 7 shows MMD when the mixed layer develops only by the surface sensible heat flux H_0. The annual variation of the MMD at Tateno were obtained by Sugiura (1972) and Hanafusa (1979). These results, excluding rainy or cloudy days, are higher than the results in Fig. 7 by 200-300 m throughout the year probably because Sugiura and Hanafusa used θ_{max} as θ_a.

Observed values of the mixed layer structure obtained by the refined direct method above Tateno or the Kanto Plain correspond comparatively well with annual variations of the mixed layer parameters, although the number of observations is small. It seems that our results represent the seasonal change of the mixed layer structure over the Kanto Plain.

Reasons for the annual change of maximum mixed layer height MMD in the march of the seasons were investigated. The mixed layer did not develop very high in midsummer because the surface heat flux H_0 was small and the lapse rate of the stable layer aloft γ was large. Conversely, MMD was highest from late winter to early spring in spite of the strong surface inversion because of a large H_0 and small γ. MMD in the autumn was not very high compared with the spring because H_0 was small and γ was not very small. MMD in winter was almost the same as that in midsummer because both values of γ and H_0 were small. We will see why H_0 shows the seasonal change in the next section, considering the heat balance of the mixed layer.

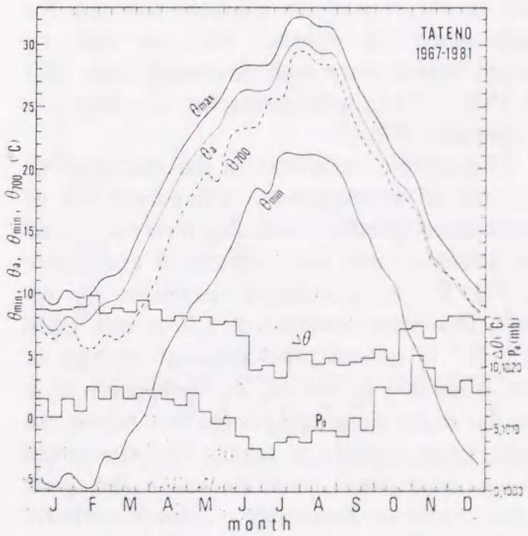

Fig. 8 Annual variations of θ_{max}, θ_a, θ_{min}, potential temperature at a height of 700 m, θ_{700} and surface pressure P_0 for days when the mixed layers are developed.

Figure 8 shows annual variations of meteorological elements θ_{max}, θ_{min}, diurnal range $\Delta\theta$, surface pressure P_0, and potential temperature θ_{700} at 700 m above the surface. The present data were obtained from the averages for fair weather days with a well developed mixed layer over a fifteen year period. In many previous researches, however, selection of fair weather days was not conducted, and various weather conditions were included in the analyzed data. Diurnal range $\Delta\theta$ was about 15°C from winter to spring, and small from June to September (10°C), $\Delta\theta$ in autumn is smaller than that in spring. From equation 4, if surface heat flux H_0 is constant throughout the seasons, as γ increases, $\Delta\theta$ becomes larger. However, this tendency is not apparent in Fig. 8 which shows H_0 varies relatively widely in season.

6. Heat balance of the mixed layer at Tateno

The downward flux of short-wave radiation and all-wave net radiation data observed by the Aerological Observatory at Tateno were analyzed to obtain the annual variation of the mixed layer structure from the viewpoint of the heat balance. Routine measurements of the net radiation have been made since 1977 and in this report we analyzed the data for days when the weather was fair and the mixed layers were well developed from 1977 to 1981. The instrumentation is shown in Fujimoto (1974).

The diurnal variations in the insolation at the top of atmosphere Q, downward flux of short-wave radiation (including direct scattered radiation) I, and net radiation R are shown in Fig. 9. In calculating insolation Q, we used the solar constant of 1.97 ly/min (1376 W/m²). In general, the seasonal change of the insolation at the top of atmosphere Q is similar to the sinusoidal curved line where the peak value appears in June. The downward flux of short-wave radiation has a flat peak from April to September. This is probably due to the large amount of water vapor and dust in the atmosphere from late spring to early autumn. On the other hand, the seasonal change in net radiation budget is very similar

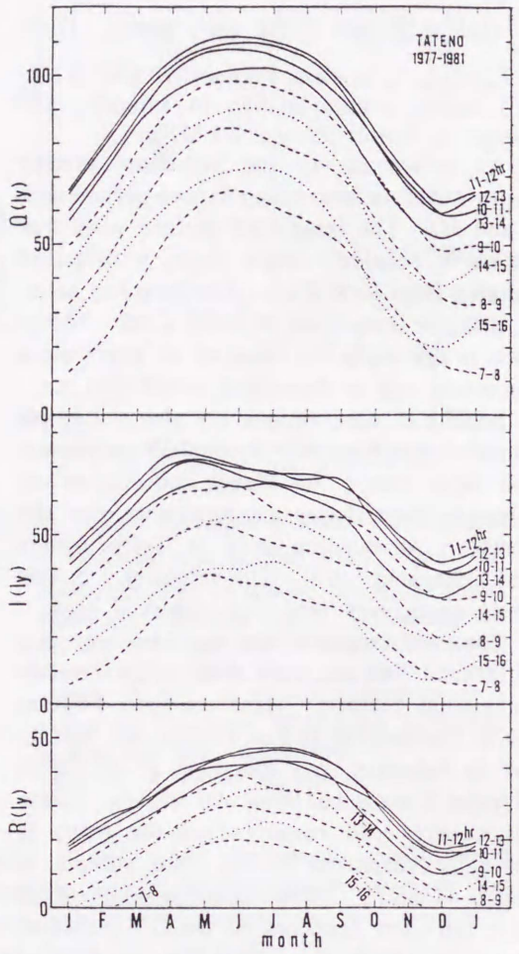

Fig. 9 Annual variations of the insolation at the top of atmosphere Q (top), the downward flux of short-wave radiation I (middle), and the net radiation R (bottom) for days when the mixed layers are developed. Data were obtained at the Tateno Aerological Observatory. 1 ly = 4.19×10^{-2} MJ/m².

to that in Q.

Annual variation of rates I/Q, R/I and R/Q at each hour are shown in Fig. 10. All three rates are nearly constant from 9–14 JST. The annual tendency of I/Q is the same as that found by Fujimoto (1974). Rate I/Q is 0.63 from June to August and 0.68 for other months. The annual variation of R/I ranges from 0.67 in July and August, to 0.41–0.46 from December to March. The value of the rate R/Q ranges from 0.25 in December to 0.43 from summer to early autumn.

Figure 11 shows the rates of integrated

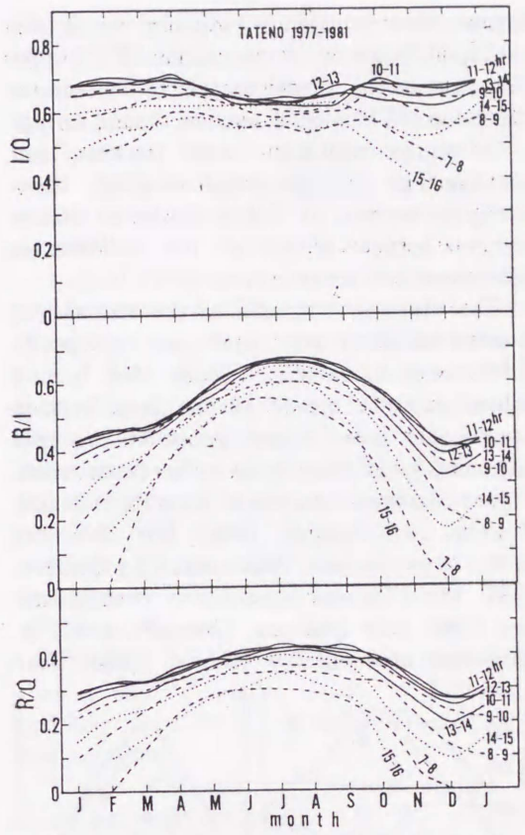

Fig. 10 Annual variations of ratios of the radiation budget components: I/Q (top), R/I (middle), and R/Q (bottom) at each hour interval at Tateno for days when the mixed layers are developed.

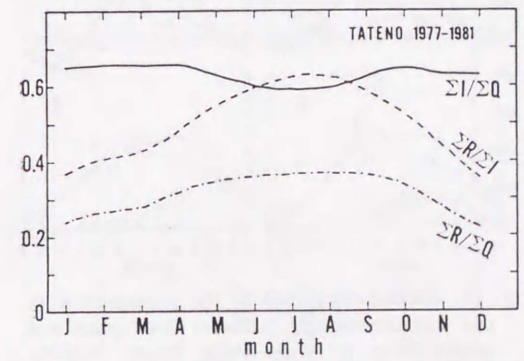

Fig. 11 Annual variations of ratios among ΣQ, ΣI and ΣR, integrated from sunrise to 13–14 JST.

values of Q, I and R from sunrise to 13–14 JST (mean values of the integral from sunrise to 13 JST and from sunrise to 14 JST). A detailed analysis shows that ratios between each integrated radiative component approaches a constant value at 11 JST and after that time the rate of growth becomes very slow. These rates have the same tendency as those in Fig. 10. This means that the contribution of radiation to the integrals of radiation in the early morning is negligible, compared to those near midday.

According to Budyko (1971), the heat transfer in a soil G is negligible when the annual range of air temperature near the ground is smaller than 10–15°C. As shown in Fig. 8, the annual range of air temperature is below 15°C at Tateno. Also, G is not large in mid-latitude districts as shown in Fig. 13. Therefore, hereafter assuming G is negligible, and that all net radiation is consumed by turbulent sensible and latent heat flux, we will see the seasonal change of the heat budget at Tateno.

Annual variations of the insolation just outside the atmosphere ΣQ, downward flux of short-wave radiation ΣI, and net radiation ΣR at Tateno are shown in Fig. 12. Each

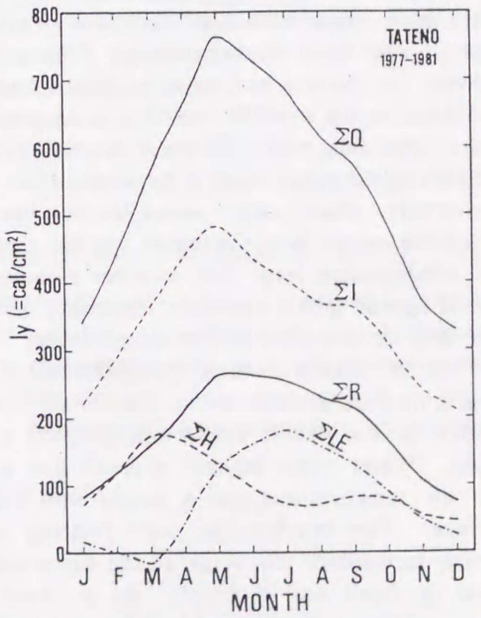

Fig. 12 Annual variations of energy balance components integrated from t_i to t_a at Tateno: ΣQ, insolation at the top of atmosphere; ΣI, downward flux of short-wave radiation; ΣR, net radiation; $\Sigma H\left(=\int_{t_i}^{t_a} H_0 dt\right)$, surface sensible heat flux; $\Sigma LE(=\Sigma R-\Sigma H)$, surface latent heat flux.

radiation component has integrated values from sunrise to t_a at which the temperature near the surface attains the maximum value θ_{max}. Integrated sensible heat flux $\int_{t_i}^{t_a} H_0 dt$ (referred to as ΣH) and integrated latent heat flux obtained by subtracting the sensible heat flux from the net radiation, ΣLE $(=\Sigma R-\Sigma H)$, are shown in the same figure.

The seasonal changes of ΣQ and ΣI have a peak value in May because the time t_a in June and July is earlier than in May by more than 30 minutes. As mentioned before, the annual variation of the sensible heat flux ΣH has double maxima and minima. The principal maximum occurs in spring and the secondary maximum in autumn, the principal minimum appears in early winter, and secondary minimum in midsummer. Latent heat flux ΣLE has one maximum in midsummer.

On fair summer days, the latent heat flux ΣLE takes on a large value, probably due to high temperatures, a large amount of evapotranspiration because the surface is covered with thick vegetation and abundant water vapor. The small air temperature difference between the surface and adjacent atmosphere also decrease the sensible heat flux in summer. Latent heat flux which does not contribute to the developing mixed layer is large in summer. Conversely, condensation levels become low. After the mixed layer becomes higher than the condensation level, fair weather cumulus clouds appear which decrease insolation and also stop development of the mixed layer.

From late winter to early spring the amount of precipitation is small, so the earth's surface is dry in the Pacific Ocean side districts of Japan. Water vapor amount is small due to low air temperatures and a nearly bare soil surface. The intensity of solar heating is similar to summer (the angle of the sun is the same in April and August). As a result, almost all net radiation seems to be converted into sensible heat flux.

In autumn, the amount of evapotranspiration decreases, but vegetation is much thicker than in spring. Although the solar heating intensity is much weaker than in spring, the air temperature near the surface is much higher than in spring (temperature at the autumnal equinox is more than 10°C higher than that at the vernal equinox). Therefore, the value of ΣH is much smaller than in spring.

In winter, insolation is the weakest, and sensible heat flux ΣH is the smallest. However, the amount of ΣH is similar to that in summer because almost all net radiation is converted into sensible heat flux.

The observed examples of the annual heat balance variation over land and rice paddy fields were examined. Figure 13-a, b, c, d shows monthly means of the heat balance components over short grass in the mid latitudes, listed from south to north latitudes. Figure 13-a was observed at West Palm Beach, Florida, USA (Sellers, 1965), Fig. 13-b was observed at Madison, Wisconsin, USA (Sellers, 1965), Fig. 13-c was observed by Frankenberger (1960) near Hanburg, Germany, and Fig. 13-d was observed by Aslyng (1960) near

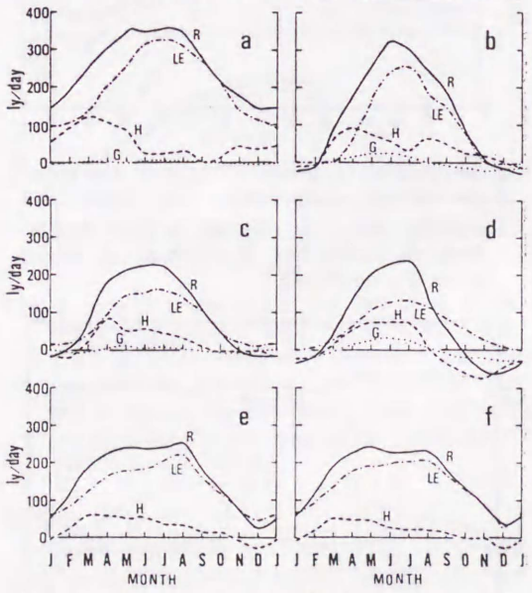

Fig. 13 Annual variations of the components of the surface energy balance over grass and paddy fields: a, West Palm Beach, Florida, USA (26.7°N); b, Madison, Wisconsin, USA (43.1°N); c, Hamburg, Germany (53.5°N); d, Copenhagen, Denmark (55.7°N); e, Mito (36.4°N); f, Kumagaya (36.2°N). R denotes the net radiation, H the sensible turbulent heat flux, LE the latent turbulent heat flux, G the transfer of heat through the ground. Data are daily totals. (1 ly/day $=4.19\times10^{-2}$ MJ/(m^2 day)).

Copenhagen, Denmark. Figures 13-e and 13-f show the heat balance over the shallow water of the paddy fields without rice plants estimated by Uchijima (1969) at Mito (60 km northeast of Tateno) and Kumagaya (80 km west of Tateno), respectively. The above results were estimated by the aerodynamic method.

Annual variation of heat balance at Wisconsin as shown in Figure 13-b, whose latitude is nearly the same as that at Tateno, has a similar heat balance variation as that at Tateno. Sensible heat flux H at Mito and Kumagaya whose positions are near Tateno is lower than that at Tateno probably due to the fact that data at Mito and Kumagaya were collected over paddy fields and all weather conditions were included. However, the tendency of the annual variation of H is similar to Tateno.

The rate $\Sigma H/\Sigma R$ is larger in our research than in other examples shown in Figure 13 probably because this research selected only fine weather.

Figure 14 shows the seasonal change of rates between integrated ΣQ, ΣI and ΣR from sunrise to t_a, and a Bowen ratio $B(\Sigma H/\Sigma LE)$. Approximately 30% and 10% of the insolation at the top of atmosphere Q is converted into sensible heat flux H, in March and August, respectively. Gamo and Yokoyama (1979) estimated $H/Q=0.2$ by comparison of the mixed layer theory and observed turbulence values. While 50% and 20% of the downward flux of short-wave radiation I is replaced in the convective sensible heat flux in March and August, respectively, the Bowen ratio B becomes unity in May and November. The lowest value of B is 0.4 in July.

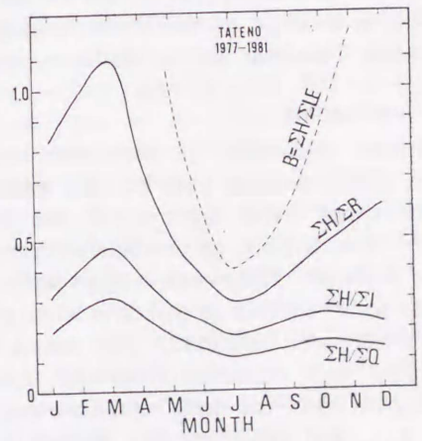

Fig. 14 Annual variations of the Bowen ratio $B(=\Sigma H/\Sigma LE)$ and ratios between $H\left(=\int_{t_i}^{t_a} H_0 dt\right)$, ΣQ, ΣI and ΣR. Values ΣQ, ΣI and ΣR are integrated values from t_i (sunrise) to t_a (time when the maximum surface temperature occurs).

7. Annual variation of turbulent structure in the mixed layer

We can estimate the turbulent velocity scale W_* in the free convection if we have a representative value of the sensible heat flux H_0. We can calculate the value of H_0 at the time t_a, H_a, in the manner described below. Let us assume that the diurnal change of the sensible heat flux H_0 is represented with a sine curve as shown in Fig. 15 as a very rough approximation and H_0 takes a zero value at sunrise t_i and sunset t_s. As the values of the integral H_0 from t_i to t_a and the times t_a and t_s are known, the value of H at $t=t_a$, H_a, is obtained by the following simple calculation. Surface sensible heat flux $H_0(s)$ in time s is calculated by

$$H_0(s)=\frac{\int_{t_i}^{t_a} H_0 dt\times10^4}{(1-\cos M)}\cdot\frac{\pi}{(t_s-t_i)}\cdot\frac{1}{60}\cdot\sin s\,,$$

where units are H_0[cal/(m^2 s)], s[rad], $\int_{t_i}^{t_a} H_0 dt$ [cal/cm^2], (t_s-t_i)[min]. M is time t_a described by a radian. The value of H_a is estimated by replacing s with M in the above equation. A free convective turbulent scale W_{*a} (W_* at t_a) is estimated from maximum mixing depth

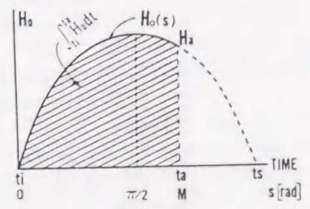

Fig. 15 Schematic figure representing the manner how to estimate the hourly variation of the sensible heat flux H_0 from the integrated one $\left(\int_{t_i}^{t_a} H_0 dt\right)$. H_a is heat flux at time t_a.

MMD and H_a from $W_*=\left(\frac{H_0}{\rho C_p}\frac{gh_m}{T_0}\right)^{1/3}$, where g is the gravity acceleration. T_0 is the mean temperature (K) within the mixed layer. According to Yokoyama *et al.* (1979), the standard deviation of the vertical velocity fluctuations σ_w at a height z is described as follows:

$$\sigma_w=C_w W_*\left(\frac{z}{h_m}\right)^{1/3}\left(1-\frac{z}{h_m}\right)^{1/3}, \quad (5)$$

where C_w is the universal constant 0.75 (Gamo *et al.*, 1983). From equation (5) σ_w reaches a maximum at a height of $h_m/2$. Therefore, σ_w at a height of MMD/2; σ_{wa} is as follows:

$$\sigma_{wa}=0.47W_{*a}.$$

Figure 16 shows the annual variations of W_{*a} and σ_{wa}. Since the meridian time H_0 is a little higher than H_a, and the mixing depth is a little lower than MMD, σ_{wa} has a similar maximum value of σ_w from around 10 to 14 JST. For comparison, σ_w selected by Yokoyama *et al.* (1979) from airborne measurements by Gamo *et al.* (1976), are shown in Figure 16. Roughly speaking, data in March and August correspond with the annual variations of σ_{wa}.

The eddy diffusivity K_m according to Yokoyama and Yoshikado (1977), is described as follows:

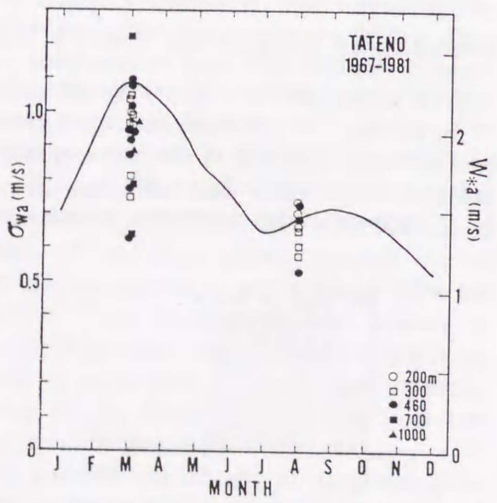

Fig. 16 Annual variations of the convective velocity scale W_{*a} (W_* at t_a), and σ_{wa} (standard deviation σ_w at a height of MMD/2 at t_a). Data are from Gamo *et al.* (1976).

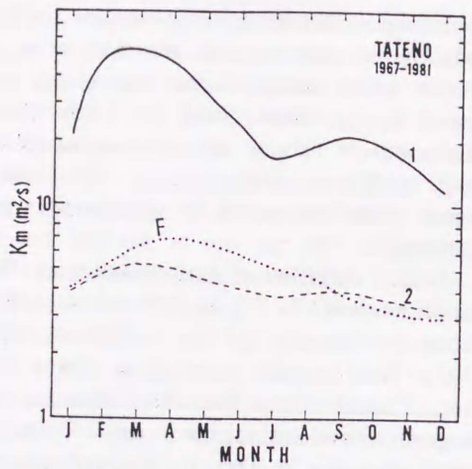

Fig. 17 Annual variations of the eddy diffusivity K_m at time t_a: 1, K_m at a height of 0.8 MMD where K_m has a peak value; 2, K_m at a height of 150 m; F, thermal diffusivity after Fig. 5 of Fujitani (1983).

$$K_m=C_{km}W_*h_m\left(1-\frac{z}{h_m}\right)^{1/3}\left(\frac{z}{h_m}\right)^{4/3}, \quad (6)$$

where C_{km} is the universal constant 0.034 from Gamo *et al.* (1983). The eddy diffusivity K_m has a peak value at $z=0.8h_m$. Line No. 1 of Fig. 17 shows the annual variation of K_m at time t_a at a height of 0.8 MMD. Line No. 2 of Fig. 17 shows K_m at a height of 150 m at time t_a. The tendencies and values of annual variations of K_m at 150 m are nearly the same as the thermal diffusivity between 100–200 m obtained by the Meteorological Observation Tower at Tateno (Fujitani, 1983).

8. Conclusions

Annual variations of maximum mixing depth MMD, sensible heat flux H_0, lapse rate of the upper stable layer above the mixed layer γ, heat balance, and turbulence quantities were obtained. Fair weather days with light winds were selected as the days when mixed layers were well developed. The mixed layer structure was estimated from the morning aerological data, the daily minimum temperature θ_{min}, and maximum θ_{max} gained by the routine measurements (profile-integrated method) over a fifteen year period from 1967 to 1981.

Here it is assumed that the first kink height of the potential temperature profile is connected with the daily minimum temperature θ_{min}, and this line is assumed to be the profile of potential temperature in the lower layer at sunrise. We assume that this modified profile of the potential temperature is destroyed by sunshine, and the mixed layer develops.

In the analysis, the following two corrections were made. First, the lag of the radiosonde thermometer was corrected. Second, the potential temperature θ_a in the mixed layer at a time when the air temperature becomes θ_{max} was assumed to be 2°C lower than θ_{max}.

The potential temperature gradient of the stable layer just above the mixed layer varies seasonally in the heights where the mixed layer develops. The value of γ is small in winter, and large in summer, γ at a height of MMD–100 m is 0.003°C/m in the winter season, 0.005 under the influence of the Ogasawara High, and 0.004 in the spring and autumn under the travelling anticyclones. The integrated surface sensible heat flux from sunrise to t_a, when the temperature becomes θ_{max}, is large in spring (170 ly) and small in summer (70 ly).

The rate of integral sensible heat flux H_0 to the integrated insolation at the top of atmosphere is 30% in spring, and 10% in summer. The surface latent heat flux obtained assuming the net radiation to be completely converted into latent and sensible heat flux is large in midsummer and low in winter. The surface sensible heat flux is large in spring due to low temperatures, a small amount of evapotranspiration, and aridity. On the other hand, in midsummer sensible heat flux is small due to moist air, high temperatures, and a large amount of evapotranspiration. That is, a great deal of net radiation is consumed in evaporation. Standard deviation of vertical velocity fluctuation and eddy diffusivity are large in spring, and small in midsummer. These results correspond with the airborne measurements.

Annual variations of the mixed layer structure estimated by the profile-integrated method agree reasonably well with observations. The profile-integrated method has been proven to be useful for analysis of the mixed layer structure as a first order estimation.

Acknowledgements

The author is grateful for data of the downward flux of short-wave radiation and net radiation from the Tateno Aerological Observatory. Thanks to Junsei Kondo, Masataka Yaji, Toshihiko Maitani, and Susumu Yamamoto for their suggestions about heat balance, Hiroaki Kondo for help with computer procedures, Hiroshi Yoshikado and Masayasu Hayashi for suggestions about weather, Osayuki Yokoyama for his criticisms, Nobuhisa Yasuda for his valuable suggestions, and Barbara J. Ishida for correcting the manuscript.

References

Budyko, M. I., 1956: The heat balance of the earth's surface. Gidrometeoizdat, Leningrad, pp. 254.

Deardorff, J. W., 1979: Prediction of convective mixed-layer entrainment for realistic capping inversion structure. *J. Atmos. Sci.*, **36**, 424-436.

Fujimoto, F., 1974: Influence of atmospheric pollution on the solar radiation measured on the ground (I). *Geophys. Mag.*, **37**, 1, 1-48.

Fujitani, T., 1983: Seasonal variations of thermal diffusivity in the atmospheric boundary layer. *Tenki*, **30**, 603-609. (in Japanese)

Fukui, E., 1977: The climate of Japan. Kodansha Limited, Tokyo, pp. 317.

Gamo, M., O. Yokoyama, S. Yamamoto and Y. Mitsuta, 1976: Structure of the atmospheric boundary layer derived from airborne measurements of the energy dissipation rate ε. *J. Meteor. Soc. Japan*, **61**, 110-124.

——— and ———, 1979: Growth of the mixing depth and the diurnal variation of vertical profiles of temperature and turbulence characteristics in the mixing layer. *J. Meteor. Soc. Japan*, **57**, 159-172.

———, S. Yamamoto, O. Yokoyama and H. Yoshikado, 1983: Structure of the free convective internal boundary layer above the coastal area. *J. Meteor. Soc. Japan*, **61**, 110-124.

———, 1983: Annual variation of the mixed layer structure at Tsukuba. *Kogai*, **18**, 294-310. (in Japanese)

Hanafusa, T., T. Fujitani and S. Otsuka, 1978: Height variation of the sensible turbulent heat flux (2). *Proc. Spring Meeting Meteor. Soc. Japan*, 121. (in Japanese)

——— and ———, 1979: Measurements of turbulence quantities in the atmospheric boundary layer. *Proc. Spring Meeting Meteor. Soc. Japan*, 145. (in Japanese)

———, 1979: Annual variation of the MMD at Tateno. Facts of the climatic variation. (ed. T. Kawamura), Kokon Shoin, Tokyo, 231-245. (in Japanese)

Holzworth, G.C., 1964: Estimations of mean maximum mixing depths in the contiguous United States. *Mon. Wea. Rev.*, **92**, 235-242.

Lee, C.B, 1983: Correction of the jump model for the mixed layer. *Proc. Autumn Meeting Meteor. Soc. Japan*, 243. (in Japanese)

——— and T. Hanafusa, 1984: Estimation of the mixed layer height by the jump model. *Proc. Spring. Meeting Meteor. Soc. Japan*, 258. (in Japanese)

Sasano, Y., I. Matsui, H. Shimizu and N. Takeuchi, 1983: Automatic determination of atmospheric mixed layer height in routine measurements by a laser radar. *J. Japan Soc. Air. Pollut*, 175-183. (in Japanese)

Sugiura, S., 1972: Max. mixing depth at Tokyo and its surroundings and correlation between relative concentration and SO_2 at Tokyo. *Tenki*, **19**, 606-612. (in Japanese)

Suzuki, Y., W. Yagihashi and S. Chubashi, 1977: Comparison of temperature, humidity and wind data between conventional rawinsonde and tethered balloon. *J. Meteor. Research*, **29**, 153-157. (in Japanese)

Uchijima. Z., 1959: A physico-climatological study of the water temperature in the paddy field. *Bull. Nat. Inst. Agr. Sci.*, **A-7**, 231-181. (in Japanese)

Willis, G.E. and J.W. Deardorff, 1974: A laboratory model of the unstable planetary boundary layer. *J. Atmos. Sci.*, **31**, 1297-1307.

Yamamoto, T., 1975: On the correction of the significant level errors due to the lag of radiosonde thermometer. *Tenki*, **22**, 671-674. (in Japanese)

Yokoyama, O., M. Gamo and S. Yamamoto, 1977: On the turbulence quantities in the atmospheric mixing layer. *J. Meteor. Soc. Japan*, **58**, 182-192.

———, ——— and ———, 1979: The vertical profiles of the turbulence quantities in the atmospheric boundary layer. *J. Meteor. Soc. Japan*, **57**, 264-272.

——— and H. Yoshikado, 1977: An aspect on the vertical profiles of wind velocity in the atmospheric boundary layer. *Bull. Nat. Res. Inst. Poll. & Res.*, **7**, 2, 1-7.

Yoshikado, H., 1980: Water channel experiment on the thermal structure of an internal boundary layer above a heated surface. *ibid*, **9**, 4, 25-34. (in Japanese)

Yoshino M., 1975: Climate in a small area. University of Tokyo Press, Tokyo, pp. 549.

筑波における混合層構造の季節変化

蒲生　稔

通商産業省公害資源研究所

館野での高層観測による温度鉛直分布，日最大および日最低気温から，地表面顕熱輸送量，最大混合層高度などの季節変化を求めた。混合層の熱収支，混合層内の乱流分布の季節変化についても解析した。上部安定層の温位勾配は冬季には 0.003°C/m，夏季には 0.005°C/m，春秋の移動性高気圧下では 0.004°C/m である。日出時から日最高気温出現時までの積算地表面顕熱輸送量は早春に 170 ly と大きく，冬季は 50 ly である。日最大混合層高度は3月に 1500 m と最高で，12月に 700 m で最低となる。早春に地表面顕熱輸送量が大きいのは，低温，乾燥，少ない蒸散活動などによるものと考えられる。ボーエン比は7月に 0.4 と最低となり，5月と11月は1である。以上の諸量は観測結果をよく説明しており，混合層構造を求める上記の簡単な方法が有効であることが確かめられた。

主論文 2

Diurnal Variations of the Mixed Layer Characteristics at Tsukuba

By Minoru Gamo

Reprinted from the Journal of the Meteorological Society of Japan
Vol. 66, No. 5, October 28, 1988

Diurnal Variations of the Mixed Layer Characteristics at Tsukuba

By Minoru Gamo

National Research Institute for Pollution and Resources, Tsukuba, Ibaraki, 305

(Manuscript received 22 July 1986, in final form 5 July 1988)

Abstract

Hourly and annual variations of the mixed layer characteristics were obtained by coupling the temperature profile of routine aerological data to near-surface hourly temperature and dew-point temperature, using a practically modified enchroachment mixed-layer model. Net radiation changes sign from minus to plus one or two hours after sunrise. This time is regarded as the effective sunrise when the mixed layer starts to develop. In most months, the mixed layer develops slowly at the beginning and then increases linearly till around noon. The Bowen ratio is unity during daytime in May. A large proportion of the net radiation is consumed by the surface latent heat flux during the summer season. During the winter season, the surface latent heat flux is larger than the surface sensible heat flux in the morning, but decreases around noon. The convective velocity scale W_* increases parabolically, and continues to increase up to early afternoon all the year.

Relative humidity has a peak value at the effective sunrise. On the other hand, specific humidity has a peak one or two hours after the effective sunrise, and after the peak it decreases gradually till 14h-15h local time due to development of the mixed layer. The diurnal patterns of the specific humidity are similar during each month, but decrease rate of the specific humidity in the daytime from July to September is small. By considering the water vapor budget in the mixed layer, the specific humidity profile in the upper stable layer at the effective sunrise is estimated.

1. Introduction

Daily variations of the mixed layer structure are important for air quality, pollutant dispersion, prediction of the temperature and humidity regimes of the small scale meteorological phenomena, etc. According to the mixed-layer theory, the mixed layer develops, entraining the upper stable layer which generally exists above the mixed layer. The potential temperature is assumed to be uniform throughout the mixed-layer because of the vertical mixing by free convection. Thus, in the mixed-layer model, particularly in the encroachment model (*e.g.*, Gamo and Yokoyama, 1979), the development of the mixed-layer and the increase of the potential temperature are simply described by the surface sensible heat flux H, and the lapse rate of the upper stable layer γ. The structure of the mixed-layer excluding about 10% of both upper and lower layers is explained by an encroachment model (Gamo *et al.*, 1983). Assuming the temperature profile of the upper stable layer, θ_u, does not change during the daytime, the hourly change of the mixed-layer characteristics is obtained by combining the early morning aerological data with hourly surface temperature data. Hourly changes of the mixed-layer height h, surface sensible heat flux H, potential temperature through the mixed-layer, θ, convective velocity scale W_* etc., are obtained. Gamo (1985) describes the representative values of the mixed-layer structure, such as

highest value of the mixed-layer h_{max} (that is, maximum mixing depth), and surface sensible heat flux integrated from sunrise to a time when the daily maximum temperature occurs. In this paper, we investigate the hourly change of the mixed-layer structure, including daily variability of energy budget parameters which are the major factors causing climatic differences of the mixed-layer characteristics.

We also consider the behavior of the water vapor in the mixed layer. Water vapor is thought of as a passive scalar quantity. However, the formation and development of convective cumulus clouds are controlled strongly by the water vapor content. For air pollution problems, the moisture characteristics are important because the water vapor is related to air pollution reactions. If a large amount of net radiation is converted into latent heat flux, it becomes inappropriate to use insolation as the parameter of the intensity of turbulence, such as in the Pasquill-Gifford stability categories. This paper discusses the diurnal course of the water vapor in the mixed layer, and estimates the diurnal change of the condensation level. In addition, taking into consideration the water vapor supply due to evaporation from the earth, and the supply due to vertical entrainment from above the mixed-layer height, the initial specific humidity profile in the early morning is evaluated.

2. Encroachment model of the mixed-layer

(1) Model for the potential temperature profile

In the present encroachment model, it is assumed that the vertical profile of the potential temperature in the stable layer over the mixed-layer does not change with time and the vertical gradient of the potential temperature, $d\theta/dz$ is zero in the mixed-layer. Basic equations of the mixed-layer are written as

$$h\frac{d\theta}{dt}=\frac{H}{\rho C_p},\quad \frac{d\theta}{dt}=\gamma\frac{dh}{dt}, \tag{1}$$

where θ is the potential temperature, h the depth of the mixed-layer, and t the time. A scheme for estimating the hourly chanes of the mixed-layer height h, and surface sensible heat flux H from around sunrise to the time when the daily temperature in the low-level atmosphere reaches its peak value is shown in Fig. 1. The mixed-layer is assumed to be instantaneously mixed. A rawinsonde is launched at 08:30JST every morning at Tateno Aerological Observatory. Therefore, the potential temperature profile around sunrise is unknown. As shown in Fig. 1, we connected the point of daily minimum temperature near the surface, θ_{min} with the lowest kink of the potential temperature profile at 08:30JST by a straight line. The vertical profile made by the above-mentioned method is assumed to be the potential temperature profile at t_I, the time when the mixed-layer starts to develop (hereafter referred to as effective sunrise), and is represented by $\theta_u(z)$. The potential temperature profile above the first kink height is assumed to be the same as the effective sunrise. Here, we assume the minimum temperature θ_{min} occurs at one or two hours after sunrise. This is because, as shown in, for example,

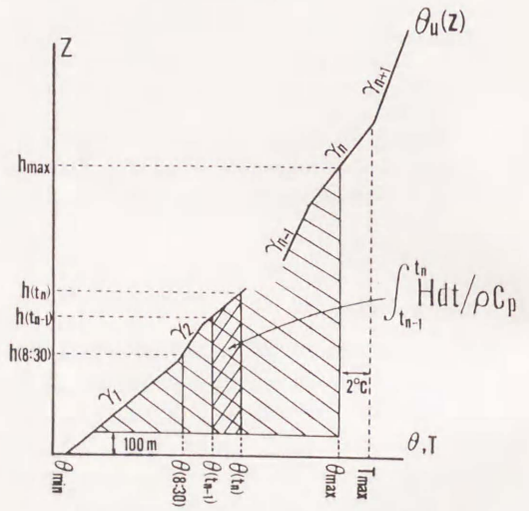

Fig. 1. The relationship between potential temperature in the mixed-layer θ, mixed-layer height h, and lapse rate γ. t_n denotes the n hrs from the effective sunrise t_I. The hatched area shows the surface heat flux supplied into the mixed layer in the time interval between t_{n-1} and t_n. θ_{min} is the temperature at t_I. (8:30) means the time when the rawinsonde is launched. T_{max}, and θ_{max} are daily maximum values of low-level temperature, and potential temperature throughout the mixed layer. h_{max} is the maximum mixing depth.

Hanafusa (1984), and Kondo and Haginoya (1985), surface sensible heat flux and net radiation do not change sign from negative to positive at sunrise, but one or two hours after sunrise. Furthermore, sensible heat flux responds almost immediately to changes of the net radiation at the surface (*e.g.* Yap and Oke, 1974). The delay times between sunrise and the time when net radiation becomes positive vary seasonally. From the net radiation data, the delay time is assumed to be one hour from May to September, and two hours from October to April.

Next, the potential temperature in the mixed-layer after 10h is assumed to be lower than the routinely observed temperature near the surface $T(^\circ C)$ by 2°C. For the time $t_n(hr)$ between the effective sunrise $t_I(hr)$ to 10h, the potential temperature in the mixed layer is assumed to be

$$T-2^\circ C\frac{t_n-t_I}{10-t_I}, \tag{2}$$

where t_n means n hours from the effective sunrise time t_I ($t_n \equiv n\text{hours}+t_I$). The above correction seems to be related to the fact that the upward decrease rate of temperature in the low-level atmosphere becomes larger with time from around sunrise to 10h. These tendencies are seen in Rayment and Reading (1974). This correction also prevents the discontinuity of temperature at the effective sunrise. A bimetal thermometer with a large time lag of about 12 seconds is attached to the rawinsonde. Thus it is assumed that rawinsonde temperature data equals the temperature at a height of 100 meters below a certain tabled altitude in the aerological data (in detail, see Gamo, 1985). A distance lag of 25 meters is assumed from March, 1981, because a bimetal thermometer with a shorter time lag of about 3-4 seconds was used from that time.

(2) Sensible and latent fluxes

As shown in Fig. 1, the area enclosed by the potential temperature profile, $\theta_u(z)$, $\theta(t_{n-1})$, and $\theta(t_n)$ (routinely measured temperature at time t_{n-1} and t_n, respectively), which is shown in the hatched area, equals $\int_{t_{n-1}}^{t_n}\{H(t)/(\rho C_p)\}dt$, the integrated surface heat flux divided by ρC_p from time t_{n-1} to time t_n. Here ρ is the air density (1.226 kgm^{-3} at 15°C), and C_p the specific heat of air (1.005×10^3 Jkg^{-1} K^{-1}).

The surface latent heat flux λE is assumed to be obtained by subtracting H from the net radiation R. That is, the value of the heat transfer in a soil, G is assumed to be very small in the following surface energy balance equation:

$$R=H+\lambda E+G \tag{3}$$

where λ is the latent heat of vaporization of water (2.466×10^6 Jkg^{-1}). Since it is difficult to fix a value of G, G is tentatively assumed to be negligibly small in this study(*). Making use of Fig. 1 and the equation (3), hourly values of mixed-layer height h, hourly integrated values of H and λE are obtained.

(3) Diurnal variation of specific humidity and trial estimation of the vertical profile of specific humidity at the effective sunrise

The specific humidity of overlying air just above the surface has a peak value at noon (*e.g.* Geiger, 1959). While the observed q behaves as at a high altitude, that is, q has a peak value in early morning and after that decreases gradually, here it is assumed that the specific humidity q calculated by routinely measured temperature and dew-point temperature is the specific humidity in the mixed-layer.

We present a model estimating the specific humidity profile in the upper stable layer at the effective sunrise, taking into consideration the budget of the water vapor in the mixed layer. That is, the diurnal variation of the moisture

(*)The value of G is a main term in the energy budget at wet surfaces such as irrigated fields (Gadda and Keers, 1970), or at dry surfaces such as deserts (Fuchs and Hadas, 1972), or above bare soil (Leuning *et al.*, 1982), or above urban areas (Oke, 1982). While there are many studies whose results show G is small, for example, about 5% of R above the usual surfaces, such as vegetation fields, and forests in the mid-latitude, according to Sugita (1984), G is small with G/R=2% above the forest canopy in Tsukuba during the summer season. Land use near the Tateno Observatory was shared by the forest (19%), grass (18%), bare soil (35%) in October (Kawashima, 1986).

content in the mixed-layer is assumed to be determined both by the addition of water vapor from the surface and by vertical convective mixing. The specific humidity q is assumed to be constant within the mixed-layer in this model. As shown in Fig. 2, we consider a slab of air including the mixed layer and the upper stable layer above a unit area ($1m^2$). Water vapor is supplied into the mixed layer by the evaporation and evapotranspiration from the surface, and at the same time by entrainment at the top of the mixed-layer from the upper stable layer. If the specific humidity in the upper stable layer is q_{u1}, and the mixed-layer increases from h_1 to h_2, and

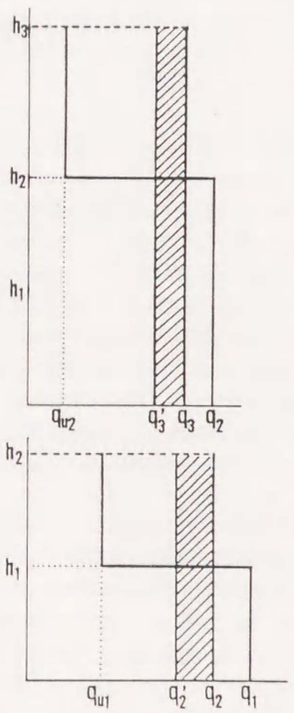

Fig. 2. Schematic figure representing the manner of estimating the specific humidity of the upper stable layer $q_{u1}\sim q_{u2}$: q, the specific humidity near the surface: h, the mixed layer height: Suffixes 1, 2, and 3 denote hours from the effective sunrise t_I, or from any time after t_I. q'_2, the specific humidity at time t_2 when there is no surface latent heat flux in the time interval between t_1 and t_2. q'_3, the specific humidity at time t_3 when there is no surface latent heat flux in the time interval between t_2 and t_3. The meshed area shows the water vapor supplied from the surface to the mixed layer by the evaporation at the surface.

the specific humidity (gkg^{-1}) becomes from q_1 to q_2 in a 1-hour interval, the following expression is derived:

$$q_1h_1+q_{u1}(h_2-h_1)=q'_2h_2\,, \tag{4}$$

where q'_2 is the specific humidity in the case where there is no surface latent heat flux, and is estimated by

$$\left(\frac{\rho}{1000}\right)(q_2-q'_2)\,h_2=\left(\frac{t_2-t_1}{\lambda}\right)(\lambda E_1)\,, \tag{5}$$

where λE_1 (Wm^{-2}) is the surface latent heat flux obtained by

$$\frac{1}{t_2-t_1}\left(\int_{t_1}^{t_2}Rdt-\int_{t_1}^{t_2}Hdt\right). \tag{6}$$

Here, $\int_{t_1}^{t_2}Rdt$ is the integrated net radiation in a 1-hour interval from t_1 and t_2. Thus, q_{u1} is derived by the equations (4)-(6), because h_1, h_2, and λE_1 are estimated by the method mentioned before, and q_1, and q_2 are known data values. Next, if the specific humidity above the layer where the specific humidity is q_{u1} is q_{u2}, as shown in Fig. 2, we have equations (4)-(6) where suffixes "1", and "2" are replaced by "2", and "3", respectively. By connecting q_{u1} with q_{u2}, we get the initial specific humidity profile at time t_1 which is eroded by free convection in the 2-hour interval between t_1 and t_3.

In general, if the condition of the mixed-layer at n hours from the effective sunrise t_I, or any time after t_I, is expressed using the subscript n, the specific humidity of the upper stable layer entrained between n hrs and n+1 hrs is expressed as follows:

$$q_{un}=(q'_{n+1}h_{n+1}-q_nh_n)/(h_{n+1}-h_n) \tag{7}$$

$$q'_{n+1}=q_{n+1}-\left(\frac{1000}{\rho}\cdot\frac{t_{n+1}-t_n}{\lambda}\right)\left(\frac{\lambda E_n}{h_n}\right), \tag{8}$$

where subscript 'n+1' denotes the value at n+1 hours after the effective sunrise t_I. Using the continuous set of the above equations obtained at every hour, the specific humidity profile at the effective sunrise $(q_{u1}, q_{u2}, \cdots, q_{un})$ can be evaluated.

(4) Condensation level

Fair weather cumulus whose scale is small, and whose life time is short, seems to appear when thermal plumes from the surface penetrate into the upper stable layer and move up higher than the lifting condensation level h_c. The value of h_c is derived by

$$h_c=(T_s-\tau_s)/(\gamma_d-\gamma_\tau)\,, \tag{9}$$

where τ is the dew-point temperature, γ_d the dry adiabatic lapse rate (0.00976 $°Cm^{-1}$), and γ_τ the dew-point temperature lapse rate. Suffix 's' denotes the value in the low-level atmosphere of the temperature and the dew-point temperature. Since γ_τ is 0.00172 ($°Cm^{-1}$) at 0°C, 0.00184 at 15°C, 0.00196 at 30°C,

$$h_c=(124.4,\ 126.2,\ 128.2)\,(T_s-\tau_s)\,, \quad (0,\ 15,\ 30°C)\,. \tag{10}$$

3. Data

An analysis was made for the five years from 1977 to 1981 at Tsukuba Science Clay (from the view point of surface characteristics, Tsukuba rural site). Usual data were measured at the Tateno Aerological Observatory located in the central section of the Tsukuba Science City. Principal site characteristics are given in Gamo (1985).

The fair-weather days with light winds, when the mixed layer was probably well developed, were selected from the routine observations at Tateno Aerological Observatory under the following three conditions. First, the duration of sunshine was longer than 75% of the maximum in the month. Second, the daily mean wind velocity was less than 3 ms^{-1}. Third, there was no daily precipitation.

Vertical profiles of temperature and relative humidity were obtained from the rawinsonde launched at 08:30 Japan Standard Time (JST). Temperature and dew-point temperature at a height of 1.5 m were measured by a Pt resistance bulb and lithium-chloride dew-point cell, respectively. Values of temperature and dew-point temperature were read from the chart recorder trace on every hour. Net radiation was calculated as the difference between upward and downward radiation (short wave and long wave radiation).

To know the hourly change of the wind speed, wind direction, and insolation duration, we used the AMeDAS (Automated Meteorological Data Aquisition System) at Shimotsuma which is located 15 km north-west of Tateno. AMeDAS data were used for the four years from 1978 to 1981, because AMeDAS data only became available from 1978. Units of wind direction, and wind speed of AMeDAS are 16 directions and (ms^{-1}), respectively. Sunshine duration indicates the cloud-free time interval duration. The value is a unity when the insolation exceeds 210 Wm^{-2} throughout the hour.

4. Results

We selected as the mixed-layer days the days when sunshine duration was over 75% of each month. However, on more cloudy days, a mixed layer also develops. Thus it seems that a typical mixed layer developed for the selected days in this paper. The number of fair-weather days for each month over the five years from 1977 to 1981 is shown below:

JAN	FEB	MAR	APR	MAY	JUN	JUL
44	37	33	35	26	17	19

AUG	SEPT	OCT	NOV	DEC
16	11	33	35	51

First, we will examine the daily patterns of general meteorological features, that is, wind speed V, wind direction D, and sunshine duration S, as the relevant meteorological conditions above the Tsukuba area (see Fig. 3). Monthly means of diurnal patterns of V, D and S are obtained from AMeDAS data at Shimotsuma.

(1) Wind speed, wind direction, and sunshine duration

Wind speed V becomes greater as the mixed layer develops. As is well known, this is because, as the mixed-layer develops, it pulls down the momentum flux of the upper stable layer where the wind is stronger than in the low-level atmosphere, and the wind speed becomes uniform in the mixed-layer. From December to March, V becomes a maximum near the time when the mixed-layer becomes highest. For other

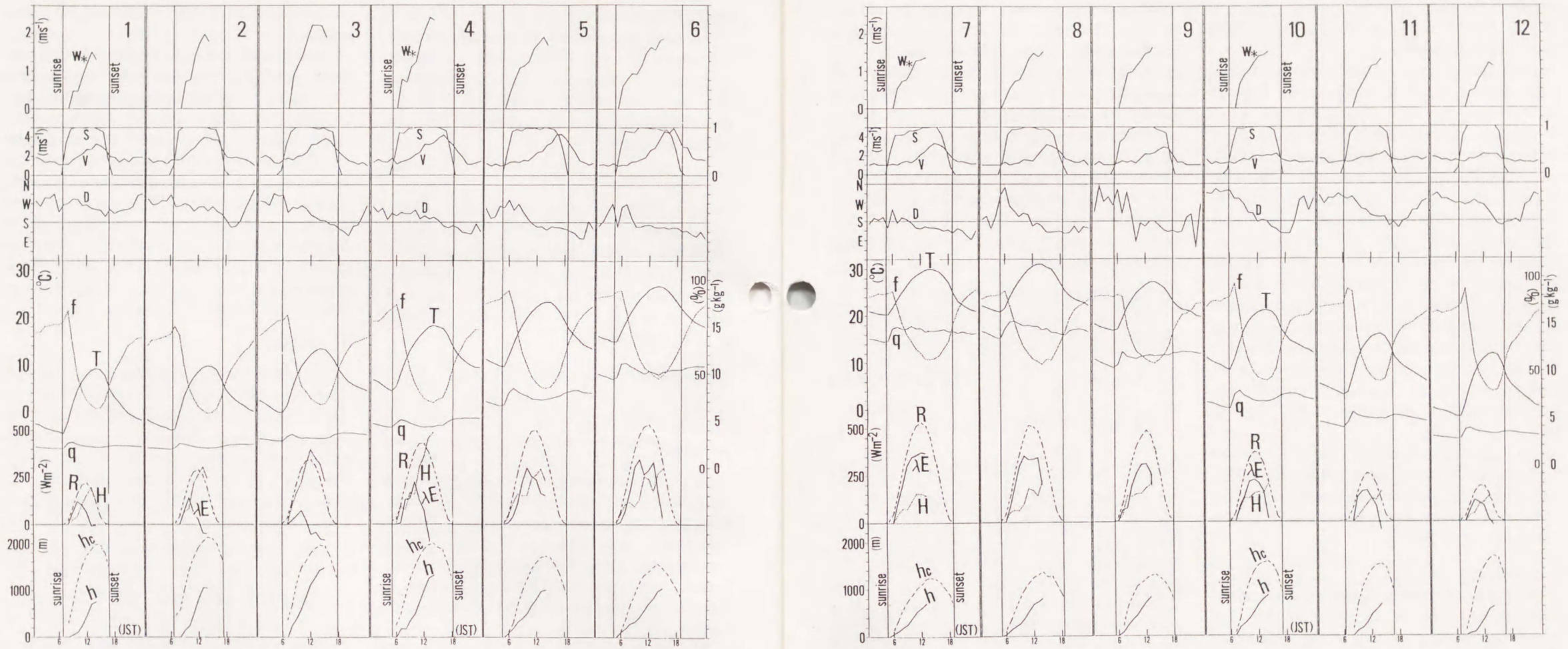

Fig. 3. Diurnal variation of the meteorological elements and the daytime trend of the mixed-layer characteristics for every month, averaged over five years from 1977 to 1981: V(ms^{-1}), wind speed (AMeDAS); D, wind direction (AMeDAS); S, duration of sunshine (AMeDAS); q(gkg^{-1}), specific humidity; f(%), relative humidity; T(°C), temperature; R(Wm^{-2}), net radiation; H(Wm^{-2}), surface sensible heat flux; λE (Wm^{-2}), surface latent heat flux; h(m), mixed layer height; h_c(m), lifting condensation level; W_*(ms^{-1}), convective velocity scale. The two vertical lines in each month show the sunrise and sunset.

months, the time when the wind speed becomes greatest is about two hours after the temperature reaches a maximum, probably because the sea breeze starts to blow.

Next, wind direction D is westerly during daytime in January and February. In other months, the westerly wind turns to southerly during daylight hours, or a southerly wind blows throughout the day. The time (hr) when wind direction becomes southerly is as follows:

MAR	APR	MAY	JUN	JUL	AUG	SEPT
15	16	12	9	14*	12	9

OCT	NOV	DEC	
11	15	15	(hr)

Except from May through October, the southerly wind starts to blow after the mixed layer reaches its maximum.

Since the weather is presumably perfectly clear when the sunshine duration S is 1.0, the variation of S in Fig. 3 shows that high insolation days are selected as the days when the typical mixed layers develop.

(*)In July the southerly wind blows through the day.

(2) Temperature

The monthly mean of the diurnal course of the temperature T averaged for five years (1977-1981) is also shown in Fig. 3. The diurnal cycle of temperature T exhibits a characteristic wave pattern. That is, the minimum temperature appears about 1 hour after sunrise, and the maximum appears in early mid-afternoon. In summer, the temperature increases even after the wind direction becomes southerly. The temperature increases rather gradually in the mixed-layer developing hours, and after T becomes maximum, the temperature decreases rather rapidly until sunset. Patterns of diurnal temperature in each month are similar to each other, but there is a seasonal variation in the absolute value, and the amplitude of diurnal wave. It is therefore meaningful to investigate the mixed-layer structure for each month.

(3) Humidity

Through the year, the relative humidity f becomes highest 1 or 2 hours after sunrise, and after its peak f decreases around midday and increases gradually again from early evening to around sunrise. Morning peak values of f are 75-90%. The peak time for f corresponds to the time when the mixed-layer starts to develop. The

minimum relative humidity around midday is 25-30% from January to March, and 55-60% from July to September.

Every month, the maximum specific humidity q is reached 2 or 3 hours after sunrise. This can be explained by the following factors. First, evaporation of dew, sublimation of frost, or evaporation of melted frost occurs. Second, evapotranspiration from soil and vegetation starts. Third, there is a possibility that the developing mixed layer entrains the upper stable layer where q is larger than in the low atmosphere, as is shown later. The specific humidity q decreases monotonically from a morning maximum value to a minimum value in the late afternoon, mainly because the mixing space becomes wide as the mixed-layer develops. The same tendency of the daily changes in the moisture is seen in Sidrov *et al.* (1984). The maximum value of q changes from 3 gkg^{-1} in January and February to 15 gkg^{-1} in July and August. The diurnal patterns of q are similar during each month, but there is little drop-off in moisture from July to September, probably because the surface latent heat flux λE is large during these months.

(4) Mixed layer height

Next, we will examine the daily pattern of the mixed-layer height h. In most months, the mixed-layer develops slowly in the early stages and after that h continues to increase linearly till around noon. Thereafter, the rate of growth of h becomes very low, and the mixed-layer becomes a maximum in the early afternoon. Especially from November to February, the speed of development of the mixed-layer is very slow in the early morning, probably because the surface stable layer is very strong. The maximum mixing depth $h_{\max}$ at Tateno is greatest in March (1,500m), rather low in mid-summer (700-800m), and lowest in December (600m). The value of $h_{\max}$ in this paper is a little lower than that given by Gamo (1985), because the instantaneous temperature is read on the hour is lower than the daily maximum temperature.

(5) Lifting condensation level

The pattern of the lifting condensation level h_c during the daytime is sinusoidal throughout the year. The difference between h_c and h is small near the effective sunrise, and after that becomes larger with time. The maximum lifting condensation level h_c is highest (2,000m) from January to April, whereas it is lowest (about 1,200m) from July to September. In all months, h_c is higher than the mixed-layer height h (around 400~1,000m). Especially from October to February, h_c is about twice as large as h, so fair-weather cumulus clouds rarely appear. This is presumably because perfectly clear days were selected for this paper.

(6) Sensible and latent heat fluxes

Next, we will discuss the daily pattern of energy fluxes at the surface. The surface sensible heat flux $H\left(=\frac{1}{t_n-t_{n-1}}\int_{t_{n-1}}^{t_n} H(t)\,dt\right)$ obtained by Fig. 1, the net radiation

$$R\left(=\frac{1}{t_n-t_{n-1}}\int_{t_{n-1}}^{t_n} R(t)\,dt\right),$$

and the latent heat flux λE, derived as the residual R-H, are also shown in Fig. 3. Net radiation R is represented with a sine curve reaching its maximum at mid-day throughout the year. As mentioned before, the net radiation becomes positive and starts to increase 1 or 2 hours after sunrise. The diurnal change of energy fluxes varies seasonally. Hourly values of H and λE are of almost the same magnitude in May. A large proportion of the net radiation is consumed in evaporation and evapotranspiration in the daytime during the summer season. These results are similar to those reported by other researchers mentioned below, althugh the sites are different. For example, Rayment and Readings (1974) observed $H/\lambda E \sim 0.5$ in May using a method similar to the one in this paper. Otaki (1984) obtained $H \sim \lambda E$ over a wheat field in May. Hicks and Wisely (1981) measured H/R=0.2 above vegetation in the midwestern United States during summer. Moores *et al.* (1979) obtained $\lambda E/R \sim 0.6$ above a grass surface in August at Cardington, England.

For the period from November to January, λE increases rather rapidly compared with H in the morning, and starts to decrease around noon, while H increases gradually up to mid-afternoon. This is probably because, after the evaporation of dew or sublimitation of frost in the morning, λE decreases owing to a small amount of water content in the soil. A similar tendency was observed in winter at Tsukuba by Zhu and Yoshino (1986). Also, from February to April, λE decreases around noon when H is the dominant term in the energy balance.

As shown in Gamo (1985), the surface sensible heat flux H shown in Fig. 3 is predominant in February and March, while λE is the dominant term in the energy balance during the summer months. Lee (1985) obtained a similar seasonal trend in energy balance terms at Tsukuba, using a sensible heat flux gained by the eddy correlation method.

(7) Convective velocity scale

Next, we will study the convective velocity scale W_* defined as $\left(\frac{H}{\rho C_p}\frac{gh}{\overline{T}}\right)^{1/3}$, where g is gravity and $\overline{T}$ (K) is the mean temperature in the mixed layer, which is a sign of the strength of the mixed layer turbulence. As shown in Fig. 3, W_* increases parabolically and continues to increase up to early afternoon all the year round. The maximum value of the daily maximum of W_* appears in spring (in March, W_* peaked at 2.2 ms^{-1}). W_* has a relatively small value in summer (in July, 1.3 ms^{-1}), as shown by Gamo (1985). A similar tendency of seasonal influence on diurnal change of W_* was observed at Tsukuba by Lee (1986).

(8) Vertical profiles of specific humidity at the effective sunrise

Fig. 4 shows the monthly means of the q profiles at the effective sunrise t_I estimated by the equations (7) and (8), where the initial time n=0 is the nearest hour from the effective sunrise. The specific humidity at the effective sunrise decreases a little in the winter, while q increases with height from April through October in the lower atmosphere layers, probably because moisture in the low-level atmosphere decreases due to dewfall during the evening and night. According to Fig. 3, the morning peak of the specific humidity appears 2 or 3 hours after sunrise, that is, 1 or 2 hours after the effective sunrise. As shown before, a reasonable explanation for this result is that the morning peak of the specific humidity can be attributed to entrainment of air above, where the specific humidity is higher than near the surface. These results are similar to Moses *et al.* (1968), where the dew-point temperature increases with height (dew-point inversion) at about sunrise. The same pattern of the specific humidity profile was observed in the Wangara data (*e.g.* Manton, 1978). It is apparent that more research is needed to confirm the specific humidity inversion, because it is not clear whether the water budget is closed in the early morning.

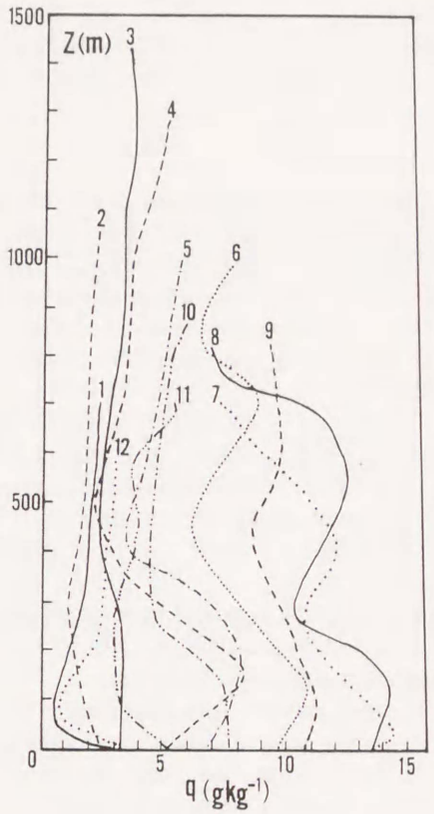

Fig. 4. Estimated monthly mean of the specific humidity profile estimated at the effective sunrise. The numbers on the profiles indicate the month.

A similar method is applied to atmospheric

pollutants in Gamo (1986), and the vertical pollutant profiles were obtained from hourly mixed-layer height and hourly surface concentration values.

5. Conclusions

Hourly and monthly variations of the mixed-layer characteristics, such as temperature, water vapor, energy budget, turbulence, mixed-layer height, lifting condensation level etc., were obtained. An analysis was made for fine days with weak wind during five years from 1977 to 1981 at Tsukuba.

The method is the extension of the method proposed by Gamo (1985), where the representative values of the mixed-layer, such as the maximum mixing depth, were obtained.

Net radiation changes sign from negative to positive 1 or 2 hours after sunrise. Here, we analyze the data assuming that the mixed layer starts to develop at a time when the net radiation changes sign (effective sunrise).

In most months, the mixed-layer develops slowly in the early morning due to the surface stable layer. After that time, the mixed-layer increases linearly till around noon. After noon, the rate of growth of h becomes very small, and mixed layer becomes a maximum in the early afternoon.

Hourly values of the surface sensible and latent heat flux in May are of almost the same magnitude during the mixed-layer developing hours. A large proportion of the net radiation is consumed in evaporation and evapotranspiration during summer season. In the winter season the surface latent heat flux increases rather rapidly in the morning, and starts to decrease around noon. This is probably because, after the evaporation of dew or the sublimation of frost in the morning, evaporation becomes small due to a small amount of water content in the soil.

The convective velocity scale W_* increases non-linearly with time, and continues to increase up to early afternoon throughout the year.

The specific humidity peaked 2 to 3 hours after the effective sunrise. After peaking, the specific humidity decreases gradually until late afternoon. By taking into account the surface latent heat flux and entrainment at the top of the mixed layer, the specific humidity profiles at the effective sunrise can be roughly estimated. The results show that the highest values of maximum of the specific humidity 2 or 3 hours after sunrise is probably due to evaporation and entrainment of the upper stable layer.

These results are similar to those by other researchers, although the sites are different. So the encroachment model which assumes that the heat and water budgets are closed in the 1-hour estimation interval seems to be confirmed to be useful. Making use of this method, climatological and diurnal features of the convective atmospheric boundary layer are able to be roughly but easily evaluated, since it requires routine standard data, or simply measured meteorological data.

Acknowledgments

The author wishes to thank Hiroshi Nishiyama and other staff of the Tateno Aerological Observatory for the temperature, dew-point temperature, and net radiation data, Hiroaki Kondo for suggestions about cloud and computer procedure, Nobuhisa Yasuda for his valuable suggestions, and Ann Chenoweth for correcting the manuscript.

References

Fuchs, M., and A. Hadas, 1972: The heat flux density in a non-homogeneous bare loessial soil. *Boundary Layer Met.*, **3,** 191-200.

Gadda A.J., and J.F. Keers, 1970: Surface exchanges of sensible and latent heat in a 10-level model atmosphere. *J.R. Met. Soc.*, **96,** 297-308.

Gamo, M., and O. Yokoyama, 1979: Growth of the mixing depth and the diurnal variation of vertical profiles of temperature and turbulence characteristics in the mixing layer. *J. Meteor. Soc. Japan,* **57,** 159-172.

———, S. Yamamoto, and O. Yokoyama, and H. Yoshikado, 1983: Structure of the free convective internal boundary layer above the coastal area. *J. Meteor. Soc. Japan,* **61,** 110-124.

———, 1985: Seasonal change of the mixed-layer structure at Tsukuba. *J. Meteor. Soc. Japan,* **63,** 60-74.

———, 1986: Diurnal and seasonal variations of pollutants in the mixed-layer. Kogai *(Pollution Control),* **21,** 129-137. (in Japanese)

Geiger, R., 1959: *The climate near the ground.* Harvard University Press.

Hanafusa, T., 1984: Analysis of atmospheric bounday layer using by MRI meteorological tower. *Tenki,* **31,** 91-100. (in Japanese)

Hicks, B.B., and M.L. Wisely, 1981: Heat and momentum transfer characteristics of adjacent fields of soybeans and maize. *Boundary Layer Met.*, **20,** 175-185.

Kawashima, S., 1986: Estimates of the surface energy balance distributions with aerial MSS data. *Tenki,* **33,** 333-344. (in Japanese)

Kondo, J. and S. Haginoya, 1985: Observational study of the transitional boundary layer. *J. Meteor. Soc. Japan,* **63,** 437-452.

Lee, C.B., 1986: Simple model and climatological aspects of the structure of the convective boundary layer. *Atmospheric Environment,* **20,** 605-714.

Leuning, R., O.T. Denmead, A.R. Lang, and E. Ohtaki, 1982: Effects of heat and water vapor transport on eddy covariance measurement of CO_2 fluxes. *Boundary Layer Met.*, **23,** 209-222.

Manton, M.J., 1978: On dry penetrative convection. *Boundary Layer Met.*, **14,** 301-322.

Moses, H., W.C. Ashby, and M.A. Bogner, 1968: Dewpoint temperature inversions. *J. Appl. Met.*, **7,** 206-216.

Moores, W.H., S.J. Caughey, C.J. Readings, J.R. Milford, D.A. Mansfield, S. Abdulla, T.H. Guymer, and W.B. Johnston, 1979: Measurements of boundary layer structure and development over SE England using aircraft and tethered balloon instrumentation. *Q.J. Roy. Met. Soc.*, 397-421.

Ohtaki, E., 1984: Application of an infrared carbon dioxide and humidity instrument to studies of turbulent transport. *Boundary Layer Met.*, **29,** 85-107.

Oke, T.R., 1982: The energetic basis of the urban heat island. *Q.J. Roy. Met. Soc.*, **108,** 1-24.

Rayment, R., and C.J. Reading, 1974: A case study of the structure and energetics of an inversion. *Q.J. Roy. Met. Soc.*, **100,** 221-233.

Sidrov, V.N., G.I. Gorchakov, A.S. Emilenko, and M.A. Sviridenkov, 1984: Diurnal course of optical and microphysical characteristics of the near-ground aerosol. *Izv. AN USSR,* **20,** 1156-1164.

Sugita, M., 1984: Energy and water balance of a pine forest during a Bai-u and a summer season. *J. Agr. Met.*, **40,** 263-269.

Yap, D. and T.R. Oke, 1974: Eddy-correction measurements of sensible heat fluxes over a grass surface. *Boundary Layer Met.*, **7,** 151-163.

Zhu, C.Q. and M. Yoshino, 1986: Diurnal change of heat balance terms and their residual term at grass land. *Environmental Research Center Papers,* **10,** 19-25. (in Japanese)

筑波における混合層特性の日変化

蒲　生　　稔

（通産省公害資源研究所）

朝の高層観測で得られた温度の鉛直分布と，ルーチン観測による地上の気温と露点温度の時間変化から，簡単な混合層モデルを使って，混合層特性の時間変化とその年変化を求めた。正味放射量は日出後１－２時間後に負から正に変わる。この時間を混合層が発達を開始する時間と見なし，有効日出時刻とした。混合層は早朝はゆっくりと発達し，その後正午ころまで直線的に増大する月が多い。ボーエン比は５月に１となり，夏季には地表面潜熱輸送量が大きい。冬季の午前中は地表面潜熱輸送量が顕熱輸送量より多いが，正午近くで急激に減少する。対流の速度スケールW_*は正午過ぎまで放物線状に増加する。

相対湿度が有効日出時刻に極大になるのに対して，比湿は有効日出時刻から１－２時間後に最大となる。比湿は最大値をとった後は混合層の発達に伴い，14－15時ころまで減少し続ける。７－９月では日中の比湿の減少割合は小さい。比湿の混合層内と，混合層に取り込まれる上部安定層内の水蒸気の収支を考慮した簡単な方法により，有効日出時刻における比湿の鉛直分布も求めてみた。

主論文3

THICKNESS OF THE DRY CONVECTION AND LARGE-SCALE SUBSIDENCE ABOVE DESERTS

M. GAMO
National Institute for Resources and Environment, Tsukuba, Ibaraki, Japan, 305

Received in final form 16 January, 1996)